PNAS RESEARCH ARTICLE | BIOCHEMISTRY OPEN ACCESS

# Evolution of nanobodies specific for BCL11A

Maolu Yin[a,b,c], Manizheh Izadi[a,b,c], Karin Tenglin[a,b,c], Thibault Viennet[d,e], Liting Zhai[f], Ge Zheng[a,b,c], Haribabu Arthanari[d,e], Laura M. K. Dassama[f], and Stuart H. Orkin[a,b,c,1]

Contributed by Stuart Orkin; received November 7, 2022; accepted December 15, 2022; reviewed by Kaiying Cheng, Shuai Qiao, Terence H. Rabbitts, and Eva-Maria Strauch

**Transcription factors (TFs) control numerous genes that are directly relevant to many human disorders. However, developing specific reagents targeting TFs within intact cells is challenging due to the presence of highly disordered regions within these proteins. Intracellular antibodies offer opportunities to probe protein function and validate therapeutic targets. Here, we describe the optimization of nanobodies specific for BCL11A, a validated target for the treatment of hemoglobin disorders. We obtained first-generation nanobodies directed to a region of BCL11A comprising zinc fingers 4 to 6 (ZF456) from a synthetic yeast surface display library, and employed error-prone mutagenesis, structural determination, and molecular modeling to enhance binding affinity. Engineered nanobodies recognized ZF6 and mediated targeted protein degradation (TPD) of BCL11A protein in erythroid cells, leading to the anticipated reactivation of fetal hemoglobin (HbF) expression. Evolved nanobodies distinguished BCL11A from its close paralog BCL11B, which shares an identical DNA-binding specificity. Given the ease of manipulation of nanobodies and their exquisite specificity, nanobody-mediated TPD of TFs should be suitable for dissecting regulatory relationships of TFs and gene targets and validating therapeutic potential of proteins of interest.**

nanobody | protein design | transcription factor | BCL11A | protein degradation

## Significance

Nuclear proteins, transcription factors (TFs), regulate many genes relevant to human diseases. Developing tools to study such TFs within intact cells is challenging. Miniature antibodies, nanobodies, are promising reagents for targeting proteins of interest to study function and/or validate therapeutic potential. We have combined several approaches, including protein design, to generate specific nanobodies that recognize TF BCL11A, a central regulator of the switch from fetal to adult-type hemoglobin. These nanobodies distinguish BCL11A from its paralog (BCL11B) and mediate targeted protein degradation of BCL11A within intact cells. These nanobodies provide opportunities for functional assessment of BCL11A and potential identification of small molecule ligands. The strategy employed here can be applied widely to target validation of other TFs within intact cells.

Single variable domains of heavy chain-only antibodies, known as nanobodies, are small polypeptides (~15 kDa) capable of stably binding their targets with high affinity. Human single-chain Fv antibody fragments (scFv) have been used for targeting proteins of interest (POIs) in intracellular antibody-capture technology (1). Both nanobodies and scFv have been employed to stabilize proteins for crystallization and structural determinations (2–7), in vivo live cell imaging of biological processes (8), and more recently as therapeutic single-domain antibodies (2). For instance, neutralizing nanobodies directed to the SARS-CoV-2 spike receptor-binding domain may be deployed for the treatment of patients with COVID-19 (9). Moreover, several procedures have been described to leverage nanobodies (or antibodies) for targeted protein degradation (TPD) through the recruitment of POIs to the proteasome (10).

Nanobodies are produced and further engineered by several approaches, most often by immunization of camelids (llama or alpaca) with cell extracts or purified proteins. This approach requires availability of live animals and accompanying animal husbandry, which is often expensive and time-consuming. As an alternative method not requiring immunization, nanobodies may be isolated from synthetic libraries (11–13). Previous efforts have sought to retrieve nanobodies by combining phage display (13, 14), yeast display (12), or ribosome display (15) with a synthetic library. Primary nanobodies obtained in this manner generally exhibit affinities for targets that are modest and insufficient for biological studies. Higher affinity nanobodies can be isolated by random limited mutagenesis (16) and structure-directed evolution (17), which is comparable to enhanced intracellular antibody capture (18). Computational affinity maturation may also be considered, in which residues in the complementary determining regions (CDRs) are altered based on the interface analysis and energy calculations (19, 20). The Rosetta software suite addressing protein structure prediction and design (21) can be used for redesign of antigen-antibody interfaces starting from existing experimental or computational models (22, 23). Taken together, a variety of strategies are available for improving the affinity of the first-generation synthetic nanobodies for specific targets.

Here, we have explored nanobodies as an aid in the characterization and targeted degradation of BCL11A, a transcriptional repressor critical in the silencing of the fetal (γ-) globin gene in the switch from fetal-to-adult hemoglobin in red cell development. To optimize BCL11A-directed nanobodies for functional studies, we combined several available methods. In the end, we report nanobodies that permit efficient TPD of BCL11A within intact cells and may also serve as tools for discovery of small molecule ligands.

Author contributions: M.Y. and S.H.O. designed research; M.Y., M.I., K.T., T.V., and L.Z. performed research; M.Y., M.I., T.V., H.A., L.M.K.D., and S.H.O. analyzed data; G.Z. contributed new reagents/analytic tools; and M.Y. and S.H.O. wrote the paper.

Reviewers: K.C., Hangzhou Normal University; S.Q., Zhejiang University; T.H.R., Institute of Cancer Research; and E.-M.S., University of Georgia.

Competing interest statement: The authors declare competing interest. Patent filing has been submitted by Boston Children's Hospital on the nanobodies reported in this manuscript.



[1]To whom correspondence may be addressed. Email: stuart_orkin@dfci.harvard.edu.

This article contains supporting information online at https://www.pnas.org/lookup/suppl/doi:10.1073/pnas.2218959120/-/DCSupplemental.

Published January 10, 2023.

## Results

**Identification of Synthetic Nanobodies Directed to BCL11A.** Full-length BCL11A protein contains a CCHC zinc finger (ZF), six regulatory C2H2 ZFs, and several disordered regions (*SI Appendix*, Fig. S1*A*). The C-terminal three ZFs (ZF456) recognize the DNA sequence TGACCA (24), which is present in the promoters of the γ-globin genes and critical for repression of γ-globin gene transcription (24, 25). The structure of this region bound to DNA reveals that ZFs four and five exhibit base contacts (26). Given the ordered nature of individual ZFs and the important functional role of ZF456 in vivo, we chose this region of BCL11A as a target for the generation of nanobodies.

To isolate candidate nanobodies, we screened a synthetic nanobody library assembled in yeast (12) against purified ZF456 protein. As shown in Fig. 1*A*, three consecutive rounds of enrichment were performed using BCL11A ZF456 protein with different epitope tags as bait. In the first two rounds, we selected potential binders by magnetic-activated cell sorting (MACS) using protein with streptavidin-binding peptide (SBP) and Flag tags, respectively. After the initial round of MACS, the positive cell population increased from ~0.7 to ~3.2% as assessed by staining with Alexa Fluor 488 (Fig. 1 *A* and *B*). Anti-flag antibody labeled with FITC was used in the second round of MACS enrichment, yielding ~4.8% of the total yeast cells in the positive pool (Fig. 1 *A* and *B*). With a subsequent round of FACS to further enrich for binders, ~9.9% of the total yeast cells in the pool displayed positive binding (Fig. 1 *A* and *B*).

After three rounds of enrichment, 96 clones were subjected to DNA sequencing. The clones were diverse. However, 14 clones were identical. Seventy-two unique clones directed against ZF456 were cloned and expressed in *Escherichia coli*; 69 were successfully purified for characterization.

Four unique clones (Nb15, Nb14, Nb53, and Nb61) scored as positive by in vitro pulldown assay with ZF456 protein (Fig. 1*C* and *SI Appendix*, Fig. S1 *A* and *B*). To confirm binding by an independent method, we examined the interaction of these nanobodies with ZF456 by NMR. Peak intensity losses were observed as expected for slow exchange regime binding. Residue-specific assignments of ZF456 were determined. All tested nanobodies bound specifically to ZF6 (Fig. 1*D* and *SI Appendix*, Fig. S2 *A* and *B*). As assessed by size exclusion chromatography, purified Nb61 and Nb53 formed stable complexes with ZF456 (*SI Appendix*, Fig. S2*C*) and were prioritized for further characterization.

**Affinity Maturation of Nanobodies by Error-Prone Mutagenesis.** The binding affinities of the primary Nbs were insufficient for the crystallization of the ZF456-Nb complex. To identify more avid Nbs, we performed error-prone PCR mutagenesis of Nb61 and Nb53 (12). Mutant libraries contained ~1 to 7 amino acid

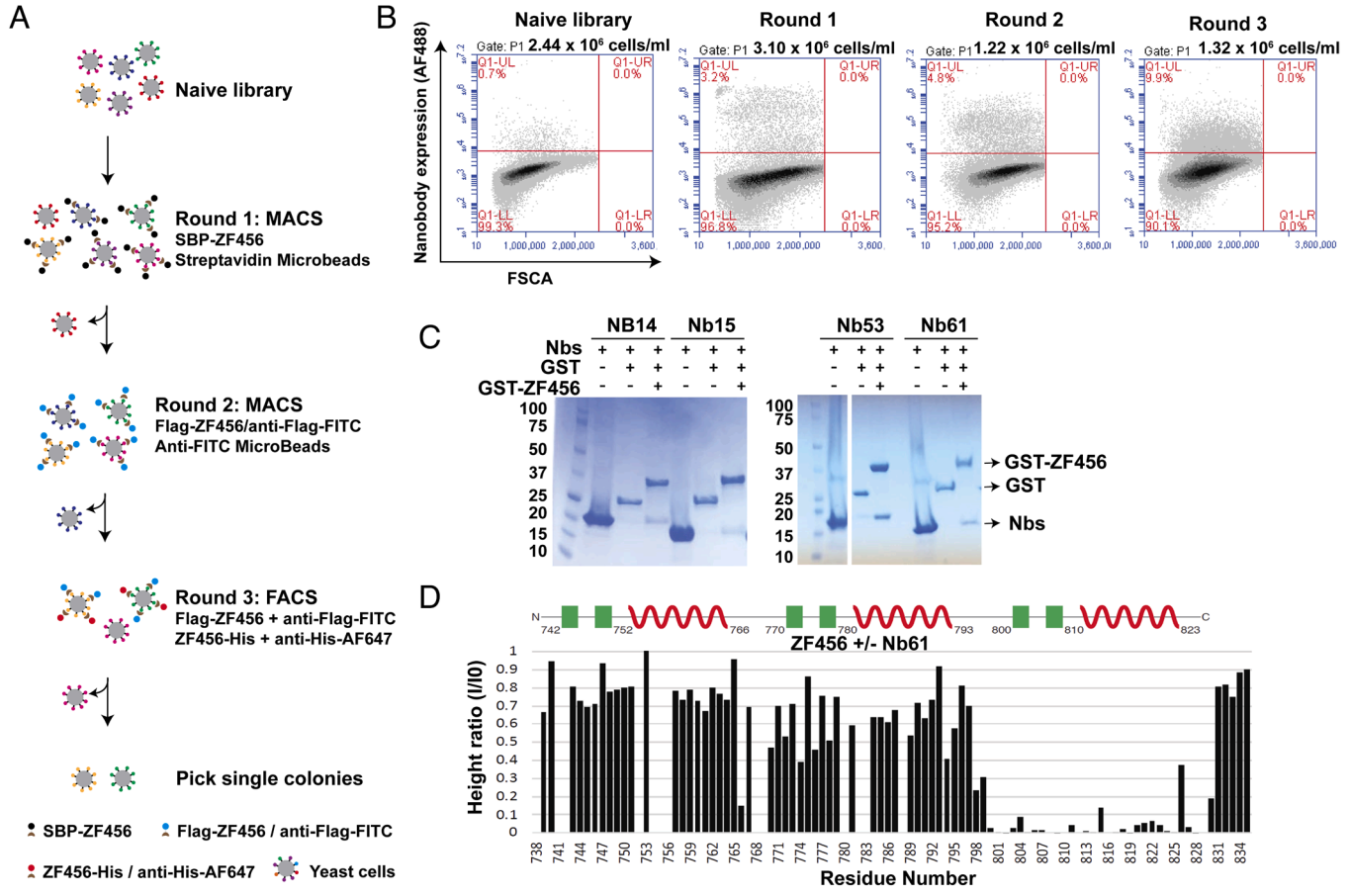


**Fig. 1.** Screen for nanobodies directed to BCL11A. (*A*) Flowchart of procedures for Nb selection. For the first round of MACS, SBP-tagged ZF456-mediated target yeast cells were isolated with streptavidin microbeads. For the second round of MACS, the cells were labeled with a mixture of flag-tagged ZF456 and anti-flag-FITC antibody, followed by selection with magnetic anti-FITC microbeads. For the third round selection, the fluorophore FITC and AF647-labeled cells were sorted by flow cytometry. (*B*) Flow cytometry plot indicating that an increased proportion of yeast interacted with ZF456 following FACS selection. (*C*) Pull-down assays confirmed four nanobodies targeting ZF456. (*D*) NMR peak intensity ratios between spectra of 1:1 ZF456:Nb61 complex and ZF456 control showing tight binding at residues 800 to 829 (values of 0 indicate unassigned residues).

substitutions per clone (*SI Appendix*, Fig. S3 *A* and *B*). High-affinity clones were enriched by one round of MACS and two rounds of FACS with streptavidin magnetic beads, AF647, and atto488, respectively (*SI Appendix*, Fig. S3*A*). Following the selection, 72 clones of mutated Nb53 and 96 clones of mutated Nb61 were subjected to DNA sequencing. (Fig. 2*A*). Ultimately, 18 clones of Nb53 and 39 clones of Nb61 were successfully expressed and purified. We identified three affinity-matured Nb61 mutants by pulldown assay. Surface plasmon resonance (SPR) confirmed that the binding affinities were improved and <700 nM (Fig. 2 *B* and *C*). Arginine 45 was mutated in all clones (Fig. 2*C*), suggesting an important contribution of this residue. The nanobodies formed a complex with ZF456 as assessed by size exclusion chromatography (Fig. 2*D*). Specificity of binding to ZF6 was confirmed by gel shift assay (Fig. 2*E*). Among the Nb53 mutants, Nb5344 exhibited the most favorable binding affinity, 3.42 ± 0.08 μM (*SI Appendix*, Fig. S4 *B* and *C*). The replacement of aspartic acid for asparagine at residue 74 further improved the binding affinity to 1.2 ± 0.05 μM (*SI Appendix*, Fig. S4 *B* and *C*).

**Evolution of Nanobodies by Structural Protein Design.** To generate nanobodies with yet higher affinity, we explored the molecular determinants of nanobody binding to ZF6 through analysis of the crystal structures of Nb6101 and Nb5344N74D bound to ZF6. Nb6101-ZF6 crystals grew in space group $P_{3121}$ and diffracted with a resolution of 2.2 Å. After determining phases using a selenomethionine solution, and performing iterative building and refinement, the structure reached an $R_{work}$/$R_{free}$ of 19.1%/23.2% (*SI Appendix*, Table S1) with four copies of the complex in an asymmetric unit. The overall structure of the Nb6101-ZF6 complex is shown in Fig. 3*A*. ZF6 laid in the backbone groove of the nanobody, while the zinc ion was oriented to the complementarity determining region 3 (CDR3) loop (Fig. 3*A* and *SI Appendix*, Fig. S4*A*). The alpha helix of ZF6 contacted the CDR2 loop and the C terminus interacted with the loops of CDR2 and CDR3 (Fig. 3*A* and *SI Appendix*, Fig. S4*A*). Ser 824, Asp 825, and Arg 826 were located in the C-terminal region after ZF6. Ser 31 and D100 in Nb6101 specifically contacted Ser 824 and Arg 826, respectively (Fig. 3*B*). Both Tyr 32 and Tyr 101 formed hydrogen bonds with Asp 825 (Fig. 3*B*). The side chain of Glu 44 in Nb6101 interacted with the side chain of Lys 801 in β-strands of ZF6 (Fig. 3*C*). There were also other interactions with the conserved residues. For instance, Tyr 37 was bound to the carbonyl group of Cys 805 in ZF6 (Fig. 3*C*). Ser 57 formed a hydrogen bond with Lys 821 in ZF6 (Fig. 3*D*). An hydrophobic interaction was present between Ile 103 and Ile 804.

The amino acid sequence of ZF456 in BCL11A is highly conserved with its paralog BCL11B (27). Nonetheless, in the region of

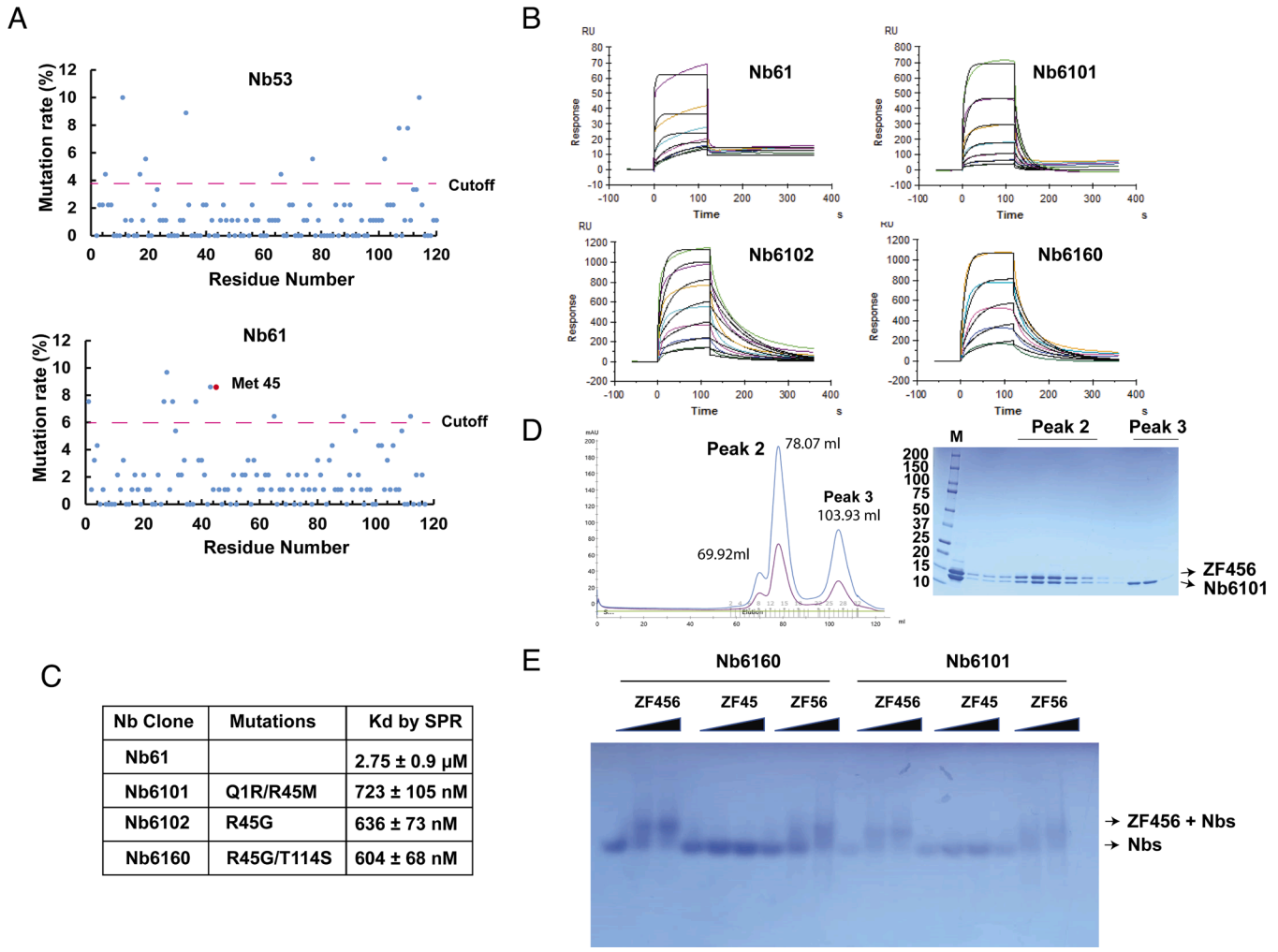


C

| Nb Clone | Mutations | Kd by SPR |
|---|---|---|
| Nb61 | | 2.75 ± 0.9 μM |
| Nb6101 | Q1R/R45M | 723 ± 105 nM |
| Nb6102 | R45G | 636 ± 73 nM |
| Nb6160 | R45G/T114S | 604 ± 68 nM |

**Fig. 2.** Affinity maturation of Nb61 and Nb53 by error-prone PCR. (*A*) Sequence analysis of randomly picked yeast colonies following MACS and FACS affinity enrichment revealed mutations that were enriched in a yeast display library generated by error-prone PCR. (*B* and *C*) SPR data showing affinity-matured variants Nb6101, Nb6102, and Nb6160 exhibited a higher affinity than Nb61. (*D*) Co-elution on the SEC column indicating Nb6101 formed a stable complex with ZF456. (*E*) Gel shift showing ZF6, but not ZF4, was essential for Nb6101 and Nb6160 binding.

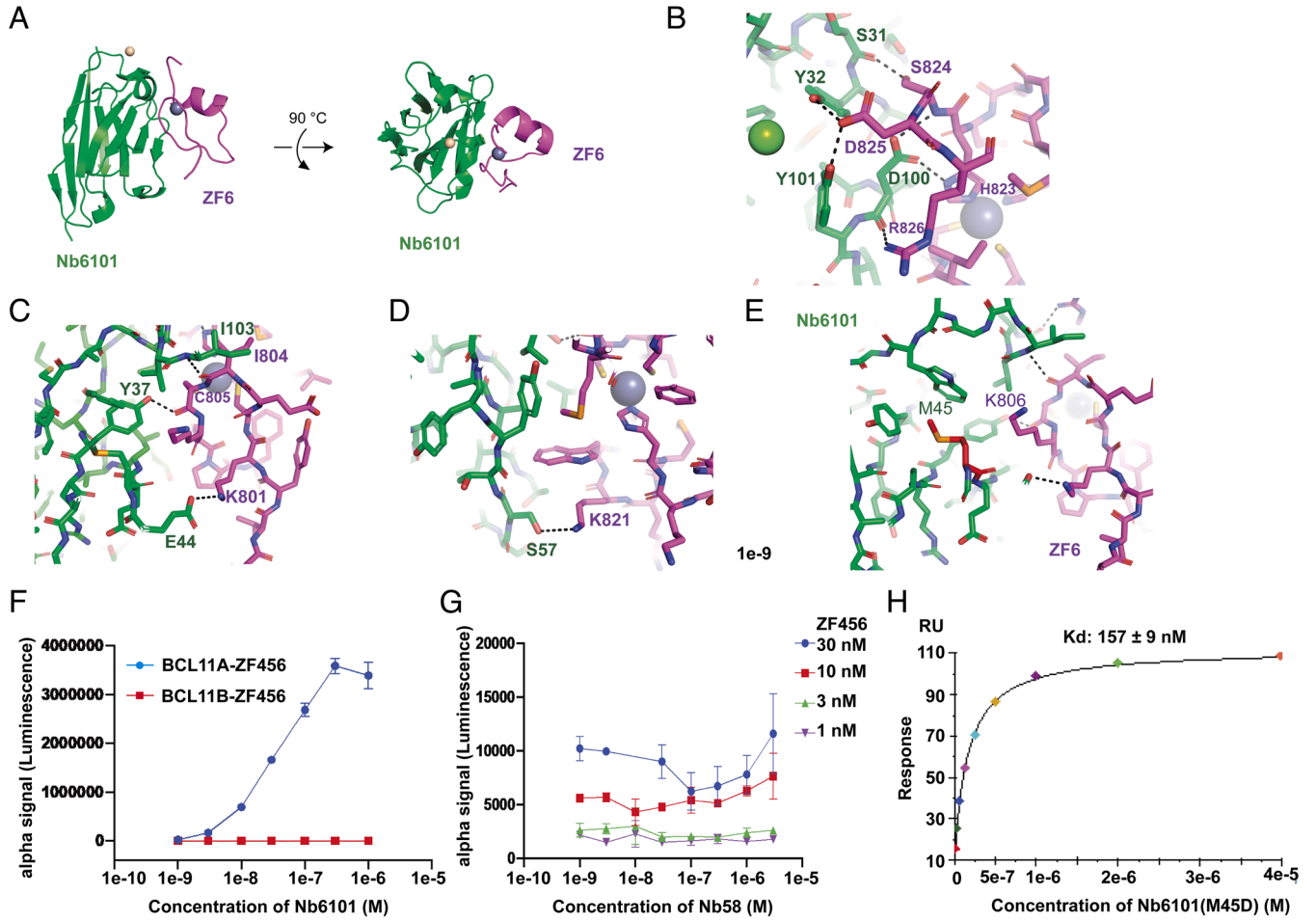


**Fig. 3.** Structural basis of Nb6101 interaction with ZF6. (*A*) The overall structure of ZF6 in complex with Nb6101. Nb6101 is shown in green and ZF6 in magenta. (*B-D*) Key residues forming interaction between Nb6101 and ZF6. (*E*) Methionine 45 in Nb6101 close to Lysine 806 in ZF6 could be replaced for potential binding enhancement. (*F*) Alpha-screen measurement revealed that Nb6101 bound to ZF456 of BCL11A but not that of BCL11B. (*G*) Negative control Nb58 did not interact with ZF456, as confirmed by the alpha-screen. (*H*) Single-cycle SPR indicating substitution of methionine 45 with aspartic improved the binding affinity.

ZF6 bound by the nanobodies, the primary sequences of BCL11A and B diverge. Consistent with the structure of nanobodies bound to BCL11A ZF6, detectable binding to ZF456 of BCL11B was not observed, as assessed by alpha-screen (Fig. 3*F*) with negative control Nb58 (Fig. 3*G*). The interaction of nanobody with the Ser 824, Asp 825, Arg 826, Lys 801, and Lys 806 via hydrogen bonds revealed the specific recognition mechanism (Fig. 3 *B–D*).

Apart from the hydrogen-bond network involving all CDRs, Met45 appeared most critical for engagement. This conclusion was consistent with the presence of residue 45 mutation in nearly all of the highly evolved nanobodies (Fig. 2*C*). Met45 was located close to Lys 806 of ZF6 but exhibited no direct interaction (Fig. 3*E*). Methionine (or glycine) at residue 45 abolished the strong positive charge clash between the original arginine in Nb61 and lysine in ZF6. To improve the binding affinity, we tested substitutions that could form hydrogen bonds with Lys806, including aspartic acid, glutamic acid, serine, and threonine. SPR measurements and gel shift assay indicated that aspartic acid replacement improved the binding affinity ~six fold (*K*d = 157 ± 9 nM) (Fig. 3*H* and *SI Appendix*, Fig. S3 *C* and *D*).

To enhance the affinity even further, we employed computational modeling and built loops before and after the ZF6 domain with a reasonable distance from the Nb6101(M45D) (Fig. 4*A*). Single-state design of the nanobody was performed with Rosetta software (https://www.rosettacommons.org/software) (28). Mutations were computationally introduced into the interaction interface, while the ZF6 domain was held constant. Approximately 76,000 models were generated and evaluated with rmsd vs. total score (Fig. 4*B*), dSASA_in vs. dG_separated (Fig. 4*C*), and Lennard-Jones attractive (*SI Appendix*, Fig. S5*A*) plots. Rmsd indicated the difference between modeled structures and the structure with the lowest energy. dSASA_int is the solvent-accessible surface area buried on the interface, and dG_separated is a change in energy of the forming complex. The top 30 models with the lowest energy and biggest interface area were selected for protein expression and purification. By an alpha-screen assay, we identified four nanobodies with substantially greater affinities, Nb6101-14 (26.7 ± 0.7 nM), Nb6101-19 (21.9 ± 0.4 nM), Nb6101-20 (77.2 ± 0.5 nM), and Nb6101-22 (54.6 ± 0.9 nM) (Fig. 4*D* and *SI Appendix*, Fig. S5*B*) with negative control Nb58 (Fig. 3*G*). The sequence alignment of the four variants showed common mutation sites, including S25D, I28D, S53A, S57Y, D100S, I103A, and D104E (*SI Appendix*, Fig. S5*C*), which may play a role in enhancing interactions.

Despite Nb5344(N74D) having a broader binding region and variability in its own CDRs, the identified crystal structure of this nanobody with ZF6 revealed a similar recognition mode (*SI Appendix*, Fig. S4*D*). Comparison of the two structures indicated that they recognized the same ZF6 epitope with few differences in the CDRs.

**Nanobody-Mediated Degradation of BCL11A and Induction of HbF Expression.** We next sought to assess the functional potential of the evolved nanobodies within intact cells for TPD of native

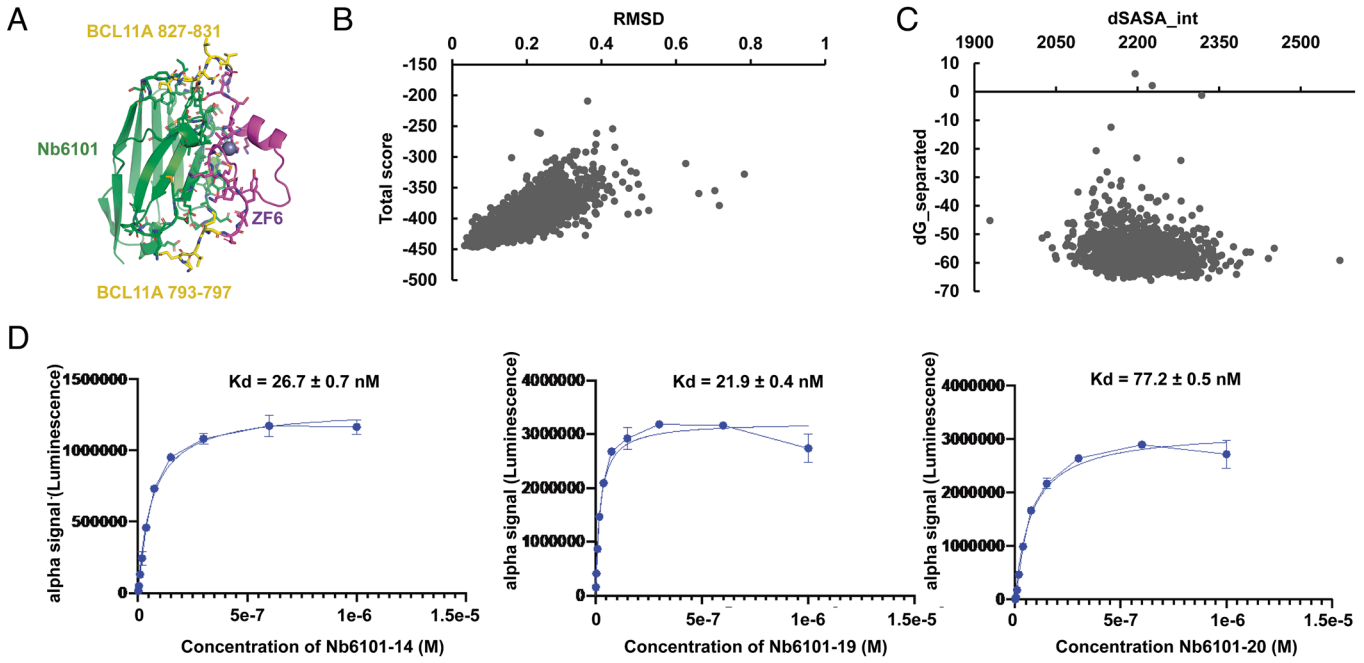


**Fig. 4.** Further evolution of Nb6101-M45D by protein design. (*A*) Loops built before and after ZF6 for Nb6101(M45D) computational evolution. (*B*) Valuation of designed models with RMSD and total score. (*C*) Valuation of designed models with the solvent accessible surface area (dSASA) buried in contact and the change in energy of the resulting complex (dG_separated). (*D*) Binding affinities of designed Nb6101 variants determined by alpha-screen.

BCL11A. Trim-Away employs antibodies (or nanobodies) and the RING E3 ligase TRIM21 to ubiquitinate non-canonical targets for degradation by the ubiquitin-proteasome (29). First, we generated TRIM21-nanobody chimeras and evaluated their potential to promote the degradation of BCL11A protein in HEK293T cells transfected with DNA constructs (*SI Appendix*, Fig. S6*A*). The expression of Nb6101-14, Nb6101-19, Nb6101-20, and Nb6101-22 conjugated with TRIM21 reduced the level of BCL11A protein, as revealed by Western blotting (Fig. 5*A*). A construct with a M10E/M72E substitution in TRIM21, which abrogates its function, was used as a control and showed no degradation (Fig. 5*A*). TRIM21 is expressed widely but not in all cells. Since TRIM21 is expressed in HEK293T cells and possesses high-affinity antibody-binding activity, we tested a construct of Nb6101-19 in fusion with an Fc domain. Fc-fusions directed BCL11A to the ubiquitin-proteasome system for disposal, as shown in Fig. 5*B* (*Right*) which demonstrates nanobody-directed TPD of BCL11A within intact cells. Alpha-screen assay revealed that Nb6101 did not bind detectably to BCL11B (Fig. 3*F*). Consistent with the structure of the nanobody-ZF6 complex, BCL11B protein is neither recognized nor degraded in the cells (Fig. 5*B*).

BCL11A acts as a highly specific and potent repressor of fetal (γ-) globin gene transcription. Human umbilical cord blood-derived erythroid progenitor-2 (HUDEP2) cells, which are immortalized human erythroid progenitor cells, serve as a convenient model of red cell differentiation and model aspects of globin gene switching. HUDEP2 cells express predominantly β-globin (and therefore, HbA, $\alpha_2\beta_2$). Upon down-regulation of BCL11A, γ-globin gene transcription is reactivated. HUDEP2 cells were transduced with lentivirus harboring Nb6101-19 fused to an Fc domain on day 0 and then cultured under differentiation conditions (*SI Appendix*, Fig. S6*B*). The level of BCL11A protein was reduced, as assayed on day 0 (Fig. 5*C*). The expression of γ-globin transcripts was increased at day 4 and day 7 (Fig. 5*D*). Fetal hemoglobin (HbF) protein level was markedly elevated on day 7 (Fig. 5*E*). In additional control experiments, we demonstrated that BCL11A protein level was unchanged in the HUDEP2 cells in which residues 724 to 835 were deleted by CRISPR/Cas9-mediated editing (Fig. 5*C*).

To examine the functional consequence of Nb6101-19-Fc fusion protein in primary cells, we used adult primary human stem and progenitor CD34+ cells. Under appropriate culture conditions, CD34+ cells differentiate along the erythroid lineage, and express largely β-globin (hence, HbA, $\alpha_2\beta_2$). The transduction of CD34+ cells with Nb6101-19-Fc fusion protein reduced the level of BCL11A protein (Fig. 5*F*) on day 0 and reactivated γ-globin expression (and HbF) on day 9 and day 12 (Fig. 5*G*). Nb6101-19 fused with Fc domain elevated HBG RNA expression and HbF protein level dramatically on day 12 of CD34+ cells differentiation compared to green fluorescent protein (GFP) and nanobody alone (Fig. 5 *G* and *H*). The percentage of HbF was increased from 2.9 to 35.2% (Fig. 5*H*).

Taken together, these findings indicate that nanobodies directed to ZF6 are functional in erythroid precursor cells for TPD of native BCL11A and reactivation of HbF.

## Discussion

Given the hierarchical and interconnected relationships of gene regulatory networks, establishing the roles of transcription factors (TFs) in specific cellular pathways, for instance, in developmental decisions and cancer, is often challenging. The knockout strategies test loss of function after a genetic manipulation and an inherent time lag, which allows for secondary consequences of TF loss and subsequent compensation. TPD offers a mean to test direct relationships between a TF and a cellular process or gene target. When a ligand has been identified for a POI, proteolysis targeting chimeras (PROTACs) represent a tractable option, although the design of an effective degrader is not straightforward and may depend on the nature and size of the linker bridging the ligand to an E3 ubiquitin ligase recruiter, as well as the specific E3 ubiquitin ligase chosen (30). A variation on the PROTAC theme, TRAFTAC, in which a DNA sequence is employed to recruit a TF, takes advantage of the high affinity of TFs for specific recognition motifs

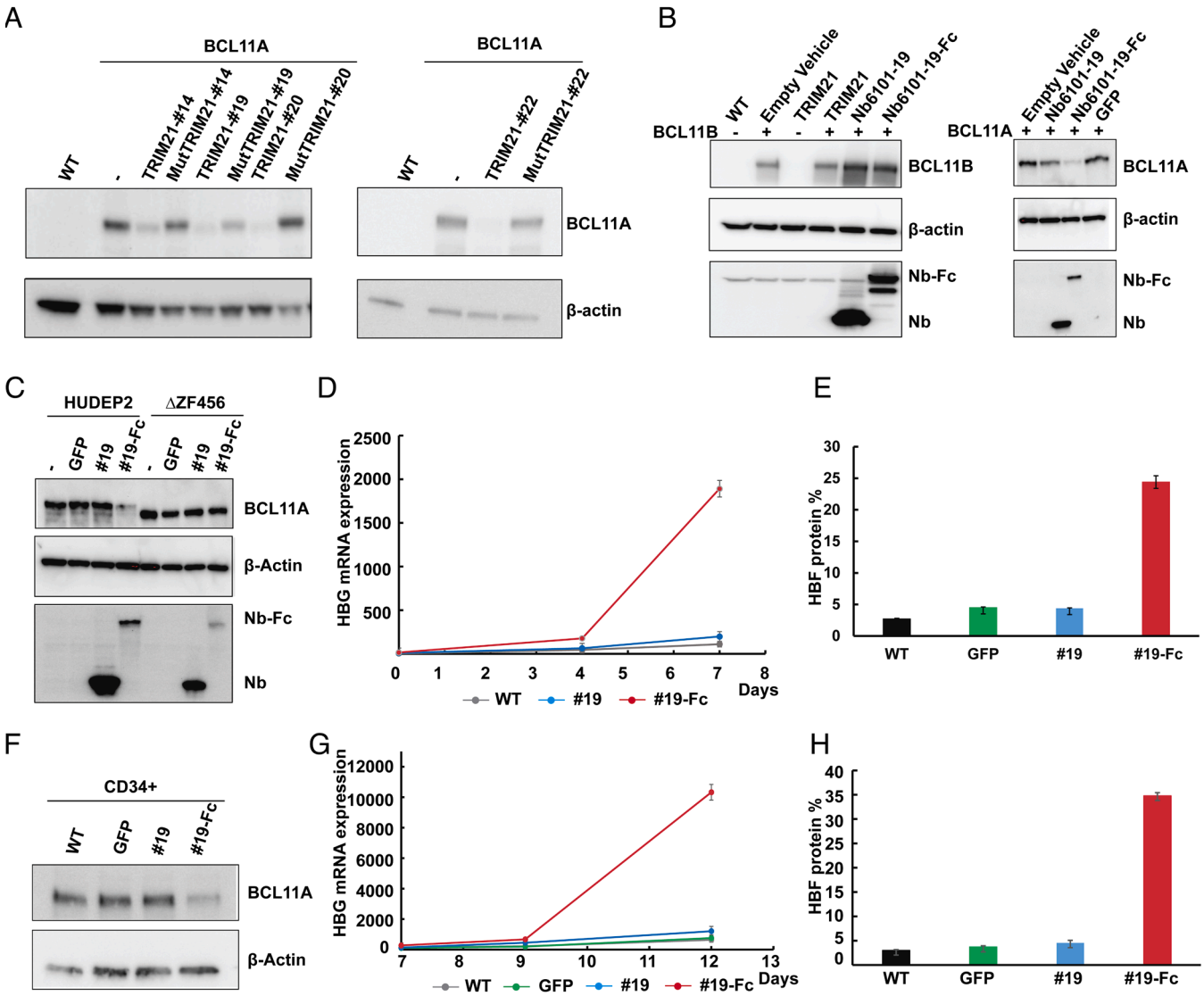


**Fig. 5.** Nanobody-mediated BCL11A degradation in HEK293T, HUDEP2 and CD34+ cells and induction of HbF expression. (*A*) Western blot indicating Nb6101-14, Nb6101-19, Nb6101-20, and Nb6101-22 fused to TRIM21 reduced the level of BCL11A protein in HEK293T cells. (*B*) Nb6101-19 fused to the Fc fragment did not induce degradation of BCL11B (*Left*), whereas BCL11A was degraded (*Right*). (*C*) Nb6101-19 fused with Fc domain reduced level of BCL11A protein in HUDEP2 cells. Deletion of ZF456 abolished nanobody-mediated degradation of BCL11A. (*D*) Induction of HBG expression by Nb6101-19 fused with Fc domain in differentiating HUDEP2 cells. (*E*) HbF protein level increased in presence of Nb6101-19 fused with Fc domain on day 7 of HUDEP2 cells differentiation compared to GFP and nanobody alone. (*F*) Nb6101-19 fused with Fc domain induced BCL11A degradation in CD34+ cells on day 0. (*G*) Induction of HBG expression by Nb6101-19 fused with Fc domain in differentiating CD34+ cells on day 7, 9, and 12. (*H*) HbF protein level dramatically increased in presence of Nb6101-19 fused with Fc domain on day 12 of CD34+ cells differentiation compared to GFP and nanobody alone.

to facilitate TPD (31, 32). However, this method relies on prior knowledge of the DNA recognition sequence for a given TF and cannot distinguish between different TFs that bind a common sequence. Therefore, the need remains for improved systems for TPD of TFs, where implementation of a PROTAC approach is limited.

With these considerations in mind, we have sought to leverage TPD for studies of BCL11A, a critical effector of HbF silencing in the red cell lineage. Preclinical studies identified BCL11A as a regulator of HbF through genome-wide association studies (33, 34), knockout experiments in mice (35), and gene editing in erythroid cells (36–39). Moreover, recent clinical trials have validated BCL11A as a therapeutic target for the reactivation of HbF in sickle cell disease and β-thalassemia (37, 40–42). Consistent with these findings, we recently employed the dTAG platform for TPD to examine the immediate consequences of BCL11A depletion on transcription and identify primary gene targets (43). Here, we sought to develop nanobodies specific for the DNA-binding region of BCL11A and deploy them for TPD. This approach allows for proteolytic degradation of BCL11A in its native form, absent of any appended tags. While commonly used tags are generally well tolerated, we observed that the addition of the variant FKBP employed in the dTAG system modestly reduced the normally long half-time (~24 h) of BCL11A to ~7.5 h (43).

We identified and optimized synthetic nanobodies that recognize one of the C-terminal ZFs of BCL11A critical for its in vivo function. Using error-prone mutagenesis, structural determination and molecular modeling, we engineered nanobodies that specifically recognize ZF6 of BCL11A in a region that is divergent from its close paralog BCL11B. The evolved nanobodies mediated the degradation of BCL11A protein in cells. Following their expression in immortalized erythroid (31) HUDEP-2 cells and primary CD34-derived erythroid cells and subsequent differentiation, nanobodies elicited increased expression of HbF comparable to that observed

with genetic down-regulation or TPD with CRISPR/Cas9 editing and the dTAG system, respectively.

Validation of POIs as targets for biological or therapeutic manipulation has most often been assessed through genetic inactivation but TPD offers an alternative means for validation. Nanobodies have specificities and affinities comparable to those of conventional antibodies and are amenable to high-throughput engineering to target diverse proteins, including TFs containing large unstructured regions. Our experiments illustrate how nanobodies may be used to modulate nuclear regulators in an approach that distinguishes closely related TFs, such as BCL11A and BCL11B, which share identical DNA-binding specificity (24). This feature distinguishes nanobody-mediated TPD from that elicited with TRAFTAC, which is based on a DNA recognition sequence (31, 32).

A potential application of intracellular antibodies in drug discovery relates to the development of small-molecule surrogates using antibody-derived (Abd) technology (44). The specific interaction interface between the antibody fragment and target protein would be mimicked by chemical compound surrogates. Chemical series identified through competition assays inside cells occupy the effector binding region and interfere with protein–protein interactions and signal transduction. The concept was initially applied in isolating drug leads directed to RAS from two commercial libraries, guided by intracellular antibodies that bind activated RAS isoforms (45, 46). Chemical surrogates that bind to LMO2 were also identified using an inhibitory intracellular antibody fragment as a competitor in a compound library screen (47). Similarly, nanobodies may be suitable for surrogate compound development in cells.

BCL11A is an extensively validated therapeutic target for HbF reactivation in sickle cell disease and β-thalassemia. While the findings reported here constitute proof-of-principle for consideration of nanobodies in treatment of the hemoglobin disorders, the implementation of this strategy would necessitate their efficient and repeated delivery to developing erythroid precursors residing in the bone marrow. With improvements in the delivery of RNA/DNA to cells in vivo (48–50), this approach could be explored further and brought to practice. Apart from any clinical application, nanobody-mediated TPD of TFs should be widely applicable as a complementary approach to genetic strategies for defining connections between regulatory factors and gene targets or pathways.

## Materials and Methods

**Cloning and Protein Purification.** DNA sequences encoding ZF456 (residues 737 to 835), ZF56 (residues 768 to 835), ZF6 (residues 797 to 826), SBP-ZF456, and Flag-ZF456 were cloned into a vector PET28a containing a N-terminal His-SUMO tag for expression in *E. coli*. Proteins were purified on a nickel column followed by cleavage of the sumo tag with Ulp1 protease. Protein was further purified on a Heparin column (Cytiva) and concentrated for nanobody screening, crystallization, SPR, pull-down assay, and gel shift assays.

Sequences encoding nanobodies for selection were cloned into vector PET26b with a C-terminal His-tag. Proteins were expressed in *Escherichia coli* and purified on a one-step NTA column. To remove imidazole, proteins were dialyzed to buffer (20 mM HEPES pH 7.5, 150 mM sodium chloride) for 2 h followed by concentration.

$^{15}$N labeled ZF456 was expressed in *Escherichia coli* in M9 medium containing 0.1% $^{15}$N-$NH_4Cl$, 0.4% glucose, 0.1 mM $CaCl_2$, 2 mM $MgSO_4$, 1 μg/mL thiamine, 50 μg/mL kanamycin, and trace element solution (1 uM $MnCl_2$, 3.1 mM $FeCl_3$, 0.62 mM $ZnCl_2$, 76 μM $CuCl_2$, 42 μM $CoCl_2$, 162 μM $H_3BO_3$, 8.1 μM $MnCl_2$). $^{15}$N-ZF456 was prepared as ZF456 except for exchanging buffer to 1 × PBS on size exclusion column (SEC).

**Isolation of Primary Nanobodies.** Nanobodies were first selected from the synthetic yeast display nanobody library (12) using MACS with streptavidin microbeads and anti-flag microbeads (Miltenyi). The enriched pool was used to select higher affinity binders by FACS sorting with anti-flag-FITC antibody and anti-his-AF647 antibody. All the MACS and FACS were performed in buffer (20 mM HEPES pH 7.5, 150 mM sodium chloride, 0.1% BSA, 1 mM DTT). After FACS selection, yeast cells were plated as single colonies which were picked and grown as clonal populations in a 96-well plate. Plasmids encoding the nanobodies were isolated with the Yeast DNA Extraction Kit (Thermo Scientific, cat# 78870) and subjected to DNA sequencing.

**Affinity Maturation of Nanobodies by Error-Prone PCR.** The affinity maturation library was prepared by assembly PCR with oligonucleotide primers (*SI Appendix*, Table S2) with the GeneMorph II Random Mutagenesis Kit (Cell Signaling Technologies, cat# 2350s). The PCR product was further amplified with primers. Mutagenic nanobody DNA and linearized pYDS649 plasmid (cut with NheI-HF and BamH1-HF) were co-electroporated into BJ5465 *S. serevisiae* cells to yield a library of transformants. Following one round of MACS and two rounds of FACS selection (*SI Appendix*, Fig. S2*A*), positive clones were enriched and sequenced. Proteins were expressed in *Escherichia coli* and validated by pull-down assay, gel shift assay, SPR, and an alpha-screen assay.

**Pull-Down Assay.** GST and GST-ZF456 protein were purified with glutathione agarose beads (Thermo Scientific Pierce) and confirmed by SDS-PAGE. 10 μM GST or GST-ZF456 was incubated with 50 μL of glutathione agarose beads in binding buffer (20 mM Tris-HCl, pH 7.5, 150 mM NaCl, and 10 μM $ZnSO_4$, and 1 mM DTT) for 30 min at room temperature. The beads were pelleted by centrifuge at 500 × g and washed twice with the binding buffer. Hundred microliters of 50 μM nanobodies were added and incubated for 30 min at 4 °C, followed by eluting with the binding buffer plus 10 μM reduced glutathione (Sigma, cat#G4251). Eluted samples were analyzed on SDS-PAGE.

**NMR.** NMR experiments were conducted on a Bruker Avance III spectrometer operating at 800 MHz, equipped with a triple-channel $^{1}$H, $^{13}$C, $^{15}$N cryogenically cooled probe. Data were processed using TopSpin (Bruker) and analyzed using CCPNmr Analysis (51).

Samples of 50 mM $^{15}$N-labeled ZnF456 (BCL11A aa 738-835) were measured in PBS buffer pH = 7.4, 1 mM dithiothreitol (DTT) and 10% v/v $^{2}H_2O$ at 25 °C. Interactions were tested in the presence of 1:1 molar equivalent of nanobodies (with or without 1.1:1 molar equivalent of 12-mer DNA).

Combined chemical shift perturbations were calculated as $[(\Delta\delta 1H)^2 + (0.102\cdot\Delta\delta 15N)^2]^{1/2}$. SD to the mean was calculated excluding outliers with values higher than 3 × SDM according to previously reported procedure (52).

**Crystallization of ZF6-Nanobody Complex.** Sequences encoding ZF6 and nanobodies were sub-cloned into the PETDuet-1 vector (Sigma-Aldrich, cat#7116) and coexpressed in *Escherichia coli* Rosetta (DE3) (Novagen). The complex was purified on a nickel column in buffer containing 20 mM Tris-HCl, pH 7.5, 150 mM NaCl, and 10 μM $ZnSO_4$. Next, the His-SUMO tag at the N terminus of ZF6 was removed by Ulp1 protease and Q column (Cytiva). Additional nanobody protein was removed from the complex on Hiload 16/600 Superdex 75 g gel filtration column (Cytiva). Samples used for crystallization were measured for final absorbance of ~50 $cm^{-1}$ using a Nanodrop spectrophotometer (Thermo Scientific). Crystals were obtained by mixing 1 μL of complex solution and 1.2 μL of reservoir solution. Crystals of ZF6-Nb6101 complex were grown from 0.1 M Bis-Tris propane, pH 6.0-7.0, 0.2 M $NaKPO_4$ and 18 to 20% PEG 3350. Crystals of ZF6-Nb5344-N74D complex were grown from 0.1 M HEPES, pH 7.5 to 8.2, 2.2M $Li_2SO_4$. All crystals were cryo-protected using corresponding reservoir buffers and flash-frozen in liquid nitrogen. Diffraction data sets were collected at the Stanford Synchrotron Radiation Lightsource. All diffraction data sets were processed with iMosflm (53). The phases of complexes were solved by the selenium single-wavelength anomalous diffraction (SAD) method using PHENIX (54). Iterative cycles of crystallographic refinement were performed using PHENIX. Coot was used for model building manually (55). All statistics of data processing and structure refinement are summarized in *SI Appendix*, Table S3. The structure figures were prepared using PyMOL (http://www.pymol.org/).

**Maturation of Nanobodies by Protein Design.** We built BCL11A loops (residue 793 to 800 and 825 to 831) around the nanobody with distance around 4 Å in the ZF6-Nb6101 complex structure using the software Coot (55). Before running a Program database (PDB) file through Rosetta (28), we removed water molecules and all ligands that were non-essential to our protocol. The residues on the nanobody–ZF6 interface were defined in the resfile file. The input complex was relaxed while restraining the atoms to their starting positions. This allowed Rosetta to relieve clashes while preventing the structure from moving too far from what was experimentally determined. Through a RosettaScripts XML file, a single round of fixed backbone design was performed. Interface residues on the nanobody were redesigned, and those on the ZF6 side were repacked. After the design step, metrics of interest were then evaluated including the score, the solvent-accessible surface buried in contact and binding energy to rank the designs and select the best models to move forward for further validation by expression of protein and affinity measurements by alpha-screen.

**SPR.** Twin-Strep-tagged ZF456 was immobilized to a single flow cell of a sensor chip CM5 (Cytivia) coated with the Strep-Tactin®XT (Twin-Strep-tag® Capture Kit, Iba, cat# 2-4370-000) using a Biacore T200 (GE Healthcare). The chip was regenerated using 3 M GuHCl. Three samples containing only running buffer, composed of 10 mM HEPES pH 7.5, 150 mM NaCl and 0.005% Tween 20, were injected over both ligand and reference flow cells, followed by nanobodies serially diluted from 7 nM to 1 μM, with a replicate of the 30 nM concentration. The resulting data were double-reference subtracted and fit to a 1:1 binding model using the Biacore T200 Evaluation software.

**Alpha-Screen Assay.** The assay was performed in 384-well plates where a constant concentration of biotinylated ZF456 protein was incubated with varying concentrations of His-tag nanobodies for 30 min at room temperature. Ten microliters of streptavidin donor beads and 10 μL of nickel chelate (Ni-NTA) acceptor beads (PerkinElmer, cat# 6760619C) in assay buffer were added and incubated in the dark for 1 h. Centrifuge for 15 s at 161 × g. The fluorescent signal was measured by a plate reader at 580 nm after excitation at 680 nM. The interaction of the two proteins brings the beads in proximity, leading to energy transfer from one bead to the other, and a burst in fluorescent signal at 520 to 620 nm which correlates with the strength of the interaction.

**Cell Culture.** Human HEK293T cells (female) were purchased from ATCC. Cells were cultured in DMEM, high glucose (Thermo Fisher Scientific, 11965) with 10% FCS and 2 mM L-Glutamine. HUDEP-2 cells (RCB4557) were obtained from Riken BioResource Research Center and cultured as reported before (56). Cells were maintained in expansion medium containing StemSpan serum-free expansion medium (SFEM, Stemcell Technologies), 2% Penicillin–Streptomycin solution (10,000 U/mL stock), 3 IU/mL Epoetin alfa (Epogen, Amgen), 0.4 μg/mL dexamethasone, 1 μg/mL doxycycline, and 50 ng/mL recombinant human stem cell factor (SCF, Stemcell Technologies). The differentiation was achieved by switching expansion medium to EDM-2 medium, which contains Iscove's modified Dulbecco's medium (IMDM), 1% L-glutamine (this is in addition to the L-glutamine present in IMDM), 2% Penicillin–Streptomycin solution (10,000 U/mL stock concentration), 330 μg/mL human holo-transferrin, 10 μg/mL recombinant human insulin solution, 2 IU/mL heparin, 5% inactivated human plasma type AB, 3 IU/mL Epoetin alfa, 100 ng/mL SCF and 1 μg/mL doxycycline. After 4 d, cells were transferred to EDM-3 medium (same as EDM-2 medium but without SCF) and cultured for another 3 d. Finally, cells were moved to EDM medium (no doxycycline) for 2 d.

Peripheral blood-derived $CD34^+$ cells were obtained from the NIDDK-Center of Excellence in Hematology at the Fred Hutchinson Cancer Research Center and cultured as described before (57). In brief, cells were cultured in erythroid differentiation medium (EDM) which contains IMDM supplemented with stabilized glutamine, 330 μg/mL holo-human transferrin, 10 ug/mL recombinant human insulin, 2 IU/mL heparin Choay, and 5% inactivated human plasma type AB. The expansion procedure comprised three phases. In the first phase (Days 0 to 7), $10^4$ /mL CD34+ cells were cultured in EDM in the presence of $10^{-6}$ M hydrocortisone (Stemcell Technologies), 100 ng/mL SCF, 5 ng/mL IL-3 (Stemcell Technologies), and 3 IU/mL Epoetin alfa. On Day 4, 1 volume of cell culture was diluted in four volumes of fresh medium containing SCF, IL-3, Epoetin alfa, and hydrocortisone. In the second phase (Days 7 to 11), the cells were resuspended at $10^5$/mL in EDM supplemented with SCF and Epo. In the third phase (Days 11 to 18), the cells were cultured in EDM supplemented with Epo alone. Cell counts were adjusted to a range of $7.5 \times 10^5$ to $1 \times 10^6$ on Day 11.

**BCL11A Degradation in HEK293T Cells.** 100K HEK293T cells were seeded in a six-well plate and transfected with 1.5 μg total amount of DNA by lipofectamine 2000 (80 ng BCL11A-HA, 800 ng Nb-Fc or Nb, and 620 ng mCherry-Trim21). Cells were sorted 24 h later followed by expanding for 48 h. 500K cells were collected for protein extraction. Forty micrograms of protein was loaded for Western blotting with anti-HA antibody (Invitrogen, cat#26183) to detect BCL11A level. The expression of fusion nanobody proteins was confirmed with anti-flag M2 antibodies (sigma, cat#F1804-50UG).

**BCL11A Degradation in Erythroid Progenitor Cell Lines.** Lentivirus particles were collected from HEK293T supernatant 3 days after cotransfection of psPAX2, VSVG, and pLVX-EF1a-IRES-Puro (Addgene, cat# 85132) plasmid constructs containing Nb6101-19 or Nb6101-19-Fc. The supernatant was filtered at 0.45 μm before storage at −80 °C. HUDPEP2 cells, ZF456 deletion HUDEP2 cells (deletion of BCL11A 724-835), and CD34+ cells were transduced with lentivirus particles at a multiplicity of ~0.1 transducing units per cell for 24 h. GFP-positive cells were sorted by flow cytometry. Protein extracted from the cells was used for Western blot with anti-BCL11A antibody (Abcam, cat#191401). RNA from differentiated HUDEP2 cells on day 0, day 4, and day 7 was prepared for quantitative RT-PCR. RNA from differentiated CD34+ cells was extracted on day 0, day 8, and day 12.

**Quantitative Reverse Transcription PCR (RT-qPCR).** Total RNA from cells was obtained with the RNeasy Plus Mini Kit (QIAGEN Cat# 74134), followed by reverse transcription to produce cDNA by using the iScript cDNA Synthesis Kit (BioRad, Cat# 1708890). Quantitative real-time PCR was performed with primers (*SI Appendix*, Table S4) and iTaq universal SYBR Green supermix (BioRad, #1725120) on a Biorad CFX384 real-time system (C1000 Touch Thermal Cycler). The level of globin transcripts was quantified by Cq values and normalized to a GAPDH internal control.

**Data, Materials, and Software Availability.** The crystallographic structure for Nb6101-ZF6 (PDB 8DTN) and Nb5344N74D-ZF6 (PDB 8DTU) has been deposited to the publicly accessible database Protein Data Bank available at https://www.rcsb.org/structure. All study data are included in the article and/or *SI Appendix*.

**ACKNOWLEDGMENTS.** We thank Prof. Andrew Kruse for the yeast display library and advice, and the HSCI-BCH flow cytometry research facility for cell sorting. Research reported in this publication was supported by R01 HL032259. S.H.O. is an Investigator of HHMI.

Author affiliations: [a]Dana Farber Boston Children's Cancer and Blood Disorders Center, Harvard Medical School, Boston, MA 02115; [b]HHMI, Harvard Medical School, Boston, MA 02115; [c]Department of Pediatrics, Harvard Medical School, Boston, MA 02115; [d]Department of Biological Chemistry and Molecular Pharmacology, Harvard Medical School, MA 02115; [e]Department of Cancer Biology, Dana-Farber Cancer Institute, MA 02215; and [f]Department of Chemistry and Sarafan ChEM-H, Stanford University, Stanford, CA 94305

1. E. Tse *et al.*, Intracellular antibody capture technology: Application to selection of intracellular antibodies recognising the BCR-ABL oncogenic protein. *J. Mol. Biol.* **317**, 85–94 (2002).
2. I. Jovcevska, S. Muyldermans, The therapeutic potential of nanobodies. *BioDrugs* **34**, 11–26 (2020).
3. A. Marturano *et al.*, Development of anti-matrix metalloproteinase-2 (MMP-2) nanobodies as potential therapeutic and diagnostic tools. *Nanomedicine* **24**, 102103 (2020).
4. C. Yu *et al.*, A nanobody targeting the LIN28: Let-7 interaction fragment of TUT4 blocks uridylation of let-7. *Proc. Natl. Acad. Sci. U.S.A.* **117**, 4653–4663 (2020).
5. M. V. Van *et al.*, Nanobody-mediated control of gene expression and epigenetic memory. *Nat. commun.* **12**, 537 (2021).
6. F. Peyvandi *et al.*, Caplacizumab reduces the frequency of major thromboembolic events, exacerbations and death in patients with acquired thrombotic thrombocytopenic purpura. *J. Thromb. Haemost.* **15**, 1448–1452 (2017).
7. H. Sewell *et al.*, Conformational flexibility of the oncogenic protein LMO2 primes the formation of the multi-protein transcription complex. *Sci. Rep.* **4**, 3643 (2014).
8. K. D. Groeve *et al.*, Nanobodies as tools for in vivo imaging of specific immune cell types. *J. Nucl. Med.* **51**, 782–789 (2010).
9. J. Huo *et al.*, Neutralizing nanobodies bind SARS-CoV-2 spike RBD and block interaction with ACE2. *Nat. Struct. Mol. Biol.* **27**, 846–854 (2020).

10. A. F. M. Ibrahim *et al.*, Antibody RING-mediated destruction of endogenous proteins. *Mol. Cell* **79**, 155–166 (2020).
11. I. Zimmermann *et al.*, Synthetic single domain antibodies for the conformational trapping of membrane proteins. *Elife* **7**, e34317 (2018).
12. C. McMahon, *et al.*, Yeast surface display platform for rapid discovery of conformationally selective nanobodies. *Nat. Struct. Mol. Biol.* **25**, 289–296 (2018).
13. S. Moutel *et al.*, NaLi-H1: A universal synthetic library of humanized nanobodies providing highly functional antibodies and intrabodies. *Elife* **5**, e16228 (2016).
14. G. P. Smith, Filamentous fusion phage: Novel expression vectors that display cloned antigens on the virion surface. *Science* **228**, 1315–1317 (1985).
15. X. Chen, M. Gentili, N. Hacohen, A. Regev, A cell-free nanobody engineering platform rapidly generates SARS-CoV-2 neutralizing nanobodies. *Nat. Commun.* **12**, 5506 (2021).
16. B. Shahi, S. L. Mousavi Gargari, I. Rasooli, M. Rajabi Bazl, R. Hoseinpoor, Random mutagenesis of BoNT/E Hc nanobody to construct a secondary phage-display library. *J. Appl. Microbiol.* **117**, 528–536 (2014).
17. S. P. Mahajan *et al.*, Computational affinity maturation of camelid single-domain intrabodies against the nonamyloid component of alpha-synuclein. *Sci. Rep.* **8**, 17611 (2018).
18. J. Zeng, H. C. Li, T. Tanaka, T. H. Rabbitts, Selection of human single domain antibodies recognizing the CMYC protein using enhanced intracellular antibody capture. *J. Immunol. Methods* **426**, 140–143 (2015).
19. D. Chaudhuri, S. Majumder, J. Datta, K. Giri, Designing of nanobodies against Dengue virus Capsid: A computational affinity maturation approach. *J. Biomol. Struct. Dyn.*, 10.1080/07391102.2022.2029773 (2022).
20. Z. Zhang, Y. Wang, Y. Ding, M. Hattori, Structure-based engineering of anti-GFP nanobody tandems as ultra-high-affinity reagents for purification. *Sci. Rep.* **10**, 6239 (2020).
21. B. Kuhlman, P. Bradley, Advances in protein structure prediction and design. *Nat. Rev. Mol. Cell Biol.* **20**, 681–697 (2019).
22. L. Cao *et al.*, Design of protein binding proteins from target structure alone. *Nature* **605**, 551–560 (2022).
23. J. Adolf-Bryfogle *et al.*, RosettaAntibodyDesign (RAbD): A general framework for computational antibody design. *PLoS Comput. Biol.* **14**, e1006112 (2018).
24. N. Liu *et al.*, Direct promoter repression by BCL11A controls the fetal to adult hemoglobin switch. *Cell* **173**, 430–442 (2018).
25. S. H. Orkin, D. E. Bauer, Emerging genetic therapy for sickle cell disease. *Annu. Rev. Med.* **70**, 257–271 (2019).
26. Y. Yang *et al.*, Structural insights into the recognition of gamma-globin gene promoter by BCL11A. *Cell Res.* **29**, 960–963 (2019).
27. S. K. Durum, Bcl11: Sibling rivalry in lymphoid development. *Nat. Immunol.* **4**, 512–514 (2003).
28. A. Leaver-Fay *et al.*, ROSETTA3: An object-oriented software suite for the simulation and design of macromolecules. *Methods Enzymol.* **487**, 545–574 (2011).
29. D. Clift *et al.*, A method for the acute and rapid degradation of endogenous proteins. *Cell* **171**, 1692–1706 (2017).
30. M. Bekes, D. R. Langley, C. M. Crews, PROTAC targeted protein degraders: The past is prologue. *Nat. Rev. Drug. Discov.* **21**, 181–200 (2022).
31. C. S. C. Ng, S. M. Banik, Taming transcription factors with TRAFTACs. *Cell Chem. Biol.* **28**, 588–590 (2021).
32. K. T. G. Samarasinghe *et al.*, Targeted degradation of transcription factors by TRAFTACs: TRAnscription factor TArgeting chimeras. *Cell Chem. Biol.* **28**, 648–661 (2021).
33. V. G. Sankaran *et al.*, Human fetal hemoglobin expression is regulated by the developmental stage-specific repressor BCL11A. *Science* **322**, 1839–1842 (2008).
34. V. G. Sankaran *et al.*, Developmental and species-divergent globin switching are driven by BCL11A. *Nature* **460**, 1093–1097 (2009).
35. J. Xu *et al.*, Correction of sickle cell disease in adult mice by interference with fetal hemoglobin silencing. *Science* **334**, 993–996 (2011).
36. M. C. Canver *et al.*, BCL11A enhancer dissection by Cas9-mediated in situ saturating mutagenesis. *Nature* **527**, 192–197 (2015).
37. H. Frangoul *et al.*, CRISPR-Cas9 gene editing for sickle cell disease and beta-thalassemia. *N. Engl. J. Med.* **384**, 252–260 (2021).
38. S. Demirci *et al.*, BCL11A enhancer-edited hematopoietic stem cells persist in rhesus monkeys without toxicity. *J. Clin. Invest.* **130**, 6677–6687 (2020).
39. J. Zeng *et al.*, Therapeutic base editing of human hematopoietic stem cells. *Nat. Med.* **26**, 535–541 (2020).
40. E. B. Esrick *et al.*, Post-transcriptional genetic silencing of BCL11A to treat sickle cell disease. *N. Engl. J. Med.* **384**, 205–215 (2021).
41. A. Basak *et al.*, BCL11A deletions result in fetal hemoglobin persistence and neurodevelopmental alterations. *J. Clin. Invest.* **125**, 2363–2368 (2015).
42. C. Brendel *et al.*, Lineage-specific BCL11A knockdown circumvents toxicities and reverses sickle phenotype. *J. Clin. Invest.* **126**, 3868–3878 (2016).
43. S. Mehta *et al.*, Temporal resolution of gene derepression and proteome changes upon PROTAC-mediated degradation of BCL11A protein in erythroid cells. *Cell Chem. Biol.* **29**, 1273–1287 (2022).
44. C. E. Quevedo *et al.*, Small molecule inhibitors of RAS-effector protein interactions derived using an intracellular antibody fragment. *Nat. Commun.* **9**, 3169 (2018).
45. T. Tanaka, T. H. Rabbitts, Intrabodies based on intracellular capture frameworks that bind the RAS protein with high affinity and impair oncogenic transformation. *EMBO J.* **22**, 1025–1035 (2003).
46. T. Tanaka, J. Thomas, R. Van Montfort, A. Miller, T. Rabbitts, Pan RAS-binding compounds selected from a chemical library by inhibiting interaction between RAS and a reduced affinity intracellular antibody. *Sci. Rep.* **11**, 1712 (2021).
47. N. Bery *et al.*, A cell-based screening method using an intracellular antibody for discovering small molecules targeting the translocation protein LMO2. *Sci. Adv.* **7**, eabg1950 (2021).
48. K. Paunovska, D. Loughrey, J. E. Dahlman, Drug delivery systems for RNA therapeutics. *Nat. Rev. Genet.* **23**, 265–280 (2022).
49. H. Faneca, Non-viral gene delivery systems. *Pharmaceutics* **13**, 446 (2021).
50. X. Pan *et al.*, Applications and developments of gene therapy drug delivery systems for genetic diseases. *Asian J. Pharm. Sci.* **16**, 687–703 (2021).
51. W. F. Vranken *et al.*, The CCPN data model for NMR spectroscopy: Development of a software pipeline. *Proteins* **59**, 687–696 (2005).
52. F. H. Schumann *et al.*, Combined chemical shift changes and amino acid specific chemical shift mapping of protein-protein interactions. *J. Biomol. NMR* **39**, 275–289 (2007).
53. T. G. Battye, L. Kontogiannis, O. Johnson, H. R. Powell, A. G. Leslie, iMOSFLM: A new graphical interface for diffraction-image processing with MOSFLM. *Acta. Crystallogr. D. Biol. Crystallogr.* **67**, 271–281 (2011).
54. D. Liebschner *et al.*, Macromolecular structure determination using X-rays, neutrons and electrons: Recent developments in Phenix. *Acta. Crystallogr. D Struct. Biol.* **75**, 861–877 (2019).
55. P. Emsley, K. Cowtan, Coot: Model-building tools for molecular graphics. *Acta. Crystallogr. D Biol. Crystallogr.* **60**, 2126–2132 (2004).
56. R. Kurita *et al.*, Establishment of immortalized human erythroid progenitor cell lines able to produce enucleated red blood cells. *PLoS One* **8**, e59890 (2013).
57. F. C. Giani *et al.*, Targeted application of human genetic variation can improve red blood cell production from stem cells. *Cell Stem Cell* **18**, 73–78 (2016).